AD-A127 556 MULTI-GRID CALCULATION OF THREE-DIMENSIONAL TRANSONIC POTENTIAL FLOWS(U) SIBLEY SCHOOL OF MECHANICAL AND AEROSPACE ENGINEERING ITHACA NY D A CAUGHEY 1982 1/1

UNCLASSIFIED N00014-77-C-0033 F/G 20/4 NL

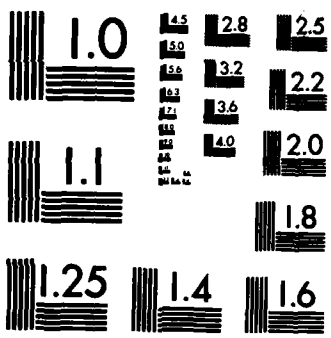

AIAA'83

AIAA-83-0374
Multi-Grid Calculation of Three-Dimensional Transonic Potential Flows

D.A. Caughey, Cornell Univ., Ithaca, NY

AIAA 21st Aerospace Sciences Meeting

January 10-13, 1983/Reno, Nevada

Unclassified

SECURITY CLASSIFICATION OF THIS PAGE (When Data Entered)

REPORT DOCUMENTATION PAGE	READ INSTRUCTIONS BEFORE COMPLETING FORM
1. REPORT NUMBER	2. GOVT ACCESSION NO. AD-A127556	3. RECIPIENT'S CATALOG NUMBER
4. TITLE (and Subtitle) Multigrid Calculation of Three-Dimensional Transonic Potential Flows	5. TYPE OF REPORT & PERIOD COVERED 6. PERFORMING ORG. REPORT NUMBER
7. AUTHOR(s) D. A. Caughey	8. CONTRACT OR GRANT NUMBER(s) N00014-77-C-0033
9. PERFORMING ORGANIZATION NAME AND ADDRESS Cornell University Mechanical and Aerospace Engineering Ithaca, N.Y. 14853	10. PROGRAM ELEMENT, PROJECT, TASK AREA & WORK UNIT NUMBERS NR 061 - 242
11. CONTROLLING OFFICE NAME AND ADDRESS Office of Naval Research Code 438 Arlington, Virginia 22217	12. REPORT DATE January 1983 13. NUMBER OF PAGES 9
14. MONITORING AGENCY NAME & ADDRESS(if different from Controlling Office) ONR Resident Representative 715 Broadway 5th Floor New York, N.Y. 10003	15. SECURITY CLASS. (of this report) Unclassified 15a. DECLASSIFICATION/DOWNGRADING SCHEDULE

16. DISTRIBUTION STATEMENT (of this Report)

Approved for public release; distribution unlimited

17. DISTRIBUTION STATEMENT (of the abstract entered in Block 20, if different from Report)

18. SUPPLEMENTARY NOTES

19. KEY WORDS (Continue on reverse side if necessary and identify by block number)

Computational Fluid Dynamics
Transonic Flow
Aerodynamics

20. ABSTRACT (Continue on reverse side if necessary and identify by block number)

A multi-grid algorithm has been developed to speed the iterative convergence of calculations for the transonic potential flow past swept wings and wing-fuselage combinations. The method is based upon a fully-conservative, finite-volume approximation to the steady potential equation which is second-order accurate everywhere in the flow field except near shock waves. The multi-grid scheme is incorporated within the framework of an alternating successive-line-overrelaxation (SLOR) solver of the

DD FORM 1 JAN 73 1473 EDITION OF 1 NOV 68 IS OBSOLETE
S/N 0102-014-6601

Unclassified

SECURITY CLASSIFICATION OF THIS PAGE (When Data Entered)

difference equations. Computed results confirm the second-order accuracy of the scheme, and demonstrate the effectiveness of the multi-grid procedure.

MULTI-GRID CALCULATION OF THREE-DIMENSIONAL TRANSONIC POTENTIAL FLOWS

D. A. Caughey[1]

Cornell University
Ithaca, New York 14853

ABSTRACT

A multi-grid algorithm has been developed to speed the iterative convergence of calculations for the transonic potential flow past swept wings and wing-fuselage combinations. The method is based upon a fully-conservative, finite-volume approximation to the steady potential equation which is second-order accurate everywhere in the flow field except near shock waves. The multi-grid scheme is incorporated within the framework of an alternating successive-line-overrelaxation (SLOR) solver of the difference equations. Computed results confirm the second-order accuracy of the scheme, and demonstrate the effectiveness of the multi-grid procedure.

I. INTRODUCTION

In the past several years, algorithms have been developed for predicting the transonic potential flow past reasonably complete aircraft configurations. In particular, the finite-volume method of Jameson and Caughey[1-3] has made it possible to calculate the transonic potential flow past any configuration for which a suitable boundary-conforming coordinate grid can be constructed. These schemes still remain quite expensive in terms of computer resources for practical use, however, primarily because of the large number of grid cells necessary for adequate resolution in three-dimensional problems and the large number of iterations required to achieve even modest convergence on these fine grids. The present paper describes work addressed primarily at this last difficulty, but also includes an improvement which addresses the first problem.

The major thrust of the current work is the incorporation of a multi-grid algorithm[4,5] to solve the difference equations. At the same time, the artificial viscosity terms have been modified to maintain almost everywhere the second-order accuracy of the original central-difference approximation used in subsonic regions of the flowfield in a manner similar to that used for two-dimensional calculations by Jameson in Reference 6. When using multi-grid to accelerate convergence in two-dimensional calculations, Jameson[7] found it necessary to use a generalized Alternating-Direction-Implicit (ADI) smoothing routine to eliminate all high wavenumber components of the error, however the results of Shmilovich and Caughey[8] and their extension to the current work demonstrates that good rates of convergence can be obtained using modified versions of the original SLOR algorithms. In order to provide reliable convergence, the bandwidth of the original SLOR scheme has been increased to allow pentadiagonal inversions along each line (instead of the tridiagonal inversions of the original scheme).

In the present paper, a brief review of the fully-conservative finite volume scheme will first be presented, concentrating upon those aspects necessary for an understanding of the improvements in the artificial viscosity, the modified SLOR schemes, and the implementation of the multi-grid algorithm. The changes resulting from the implementation of the new features will then be described, and results indicating the improved iterative convergence and accuracy of the new scheme will be presented. A comparison of results calculated using the original first-order accurate and new second-order accurate schemes will also provide some guidelines on the number of mesh points required for given levels of accuracy in force coefficients for these three-dimensional calculations.

II. ANALYSIS

The current work is based upon the finite-volume method of Jameson and Caughey.[1-3] That method provides a discrete approximation to the nonlinear potential equation of transonic flow which may be interpreted either as a finite-difference method which balances fluxes across cell faces or as a finite element method based upon the Bateman variational principle. In the original formulation of that method, a first-order truncation error was introduced by the addition of an artificial viscosity needed to stabilize the scheme in regions of supersonic flow, and the difference equations were solved by an SLOR scheme.

A. Finite-Volume Formulation

Many aerodynamic problems of practical interest, including transonic flows with weak shock waves, can be usefully approximated as potential and steady. In strong conservation form, the equation for the velocity potential ϕ can be written in Cartesian coordinates (x,y,z) as

$$(\rho\phi_x)_x + (\rho\phi_y)_y + (\rho\phi_z)_z = 0, \qquad (1)$$

[1]Associate Professor, Sibley School of Mechanical and Aerospace Engineering. Member, AIAA.

where ρ is the density, given by the isentropic law

$$\rho = \{1 + (\gamma-1)/2\ M_\infty^2(1 - q^2)\}^{1/(\gamma-1)} \qquad (2)$$

Here M_∞ is the Mach number of the free stream, q is the magnitude of the velocity $\nabla\phi$, and the density and velocity have been normalized by their freestream values.

The finite-volume method for transonic potential flow[1-3] is a geometrically-general technique based upon a numerical evaluation of the transformation metrics produced by an arbitrary transformation to boundary-conforming coordinates. Consider a transformation to a new set of coordinates X,Y,Z. Let the Jacobian matrix of the transformation be defined by

$$H = \begin{Bmatrix} x_X & x_Y & x_Z \\ y_X & y_Y & y_Z \\ z_X & z_Y & z_Z \end{Bmatrix} , \qquad (3)$$

and let h denote the determinant of H. The metric tensor of the new coordinate system is given by the matrix $G = H^T H$, and the contravariant components of the velocity vector U, V, and W are given by

$$\begin{Bmatrix} U \\ V \\ W \end{Bmatrix} = H^{-1} \begin{Bmatrix} u \\ v \\ w \end{Bmatrix} = G^{-1} \begin{Bmatrix} \phi_X \\ \phi_Y \\ \phi_Z \end{Bmatrix} . \qquad (4)$$

Eq.(1), upon multiplication by h, can then be written

$$(\rho hU)_X + (\rho hV)_Y + (\rho hW)_Z = 0. \qquad (5)$$

The fully-conservative, finite-volume approximation corresponding to Eq.(5) is constructed by assuming separate trilinear variations of the independent and dependent variables within each mesh cell.

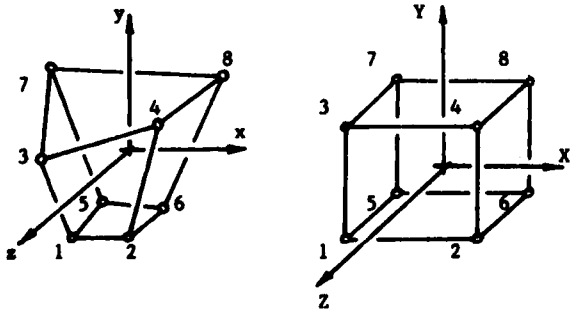

(a) Physical cell (b) Computational cell

Figure 1. Mapping of mesh cells.

Numbering the cell vertices as illustrated in Figure 1, and assuming that the local coordinates $X_i = \pm 1/2$, $Y_i = \pm 1/2$, $Z_i = \pm 1/2$ at the vertices, the local mapping can be written

$$x = 8\sum_{i=1}^{4} x_i(1/4 + X_i X)(1/4 + Y_i Y)(1/4 + Z_i Z). \qquad (6)$$

Similar formulas hold for y, z and ϕ. If we introduce the averaging and differencing operators

$$\begin{aligned} \mu_X f_{i,j,k} &= 1/2(f_{i+1/2,j,k} + f_{i-1/2,j,k}) \\ \delta_X f_{i,j,k} &= (f_{i+1/2,j,k} - f_{i-1/2,j,k}) \end{aligned} \qquad (7)$$

then the transformation dervivatives, evaluated at the cell centers, can be expressed by formulas such as

$$\begin{aligned} x_X &= \mu_{YZ}\delta_X x, \\ x_Y &= \mu_{XZ}\delta_Y x, \\ x_Z &= \mu_{XY}\delta_Z x, \end{aligned} \qquad (8)$$

with similar expressions for the derivatives of y, z and the potential. Such formulas can be used to determine ρ, h, U, V, and W at the center of each cell using Eqs.(2),(3), and (4). Eq.(5) is represented by conserving fluxes across the boundaries of auxiliary cells whose faces are chosen to be midway between the faces of the primary mesh cells. This can be represented as

$$\mu_{YZ}\delta_X(\rho hU) + \mu_{XZ}\delta_Y(\rho hV) + \mu_{XY}\delta_Z(\rho hW) = 0. \qquad (9)$$

This formula can also be obtained by applying the Bateman variational principle that the integral of the pressure

$$I = \int p\ dx\ dy\ dz \qquad (10)$$

is stationary, and approximating I by a simple one-point integration scheme in which the pressure at the center of each grid cell is multiplied by the cell volume. In this way, for subsonic flow, the finite-volume method can equally well be regarded as a finite element method with isoparametric trilinear elements.

The use of the one-point integration scheme leading to Eq.(9) has the advantage of requiring only one density evaluation per mesh point, but also has the undesirable effect of tending to decouple the solution at odd- and even-numbered points of the grid, and suitable recoupling terms can be added to improve the stability of the solution.

We define

$$\begin{aligned} T = -\frac{\rho}{2}\{&\mu_Z\delta_{XY}(A_X + A_Y)\mu_Z\delta_{XY} \\ &+ \mu_X\delta_{YZ}(A_Y + A_Z)\mu_X\delta_{YZ} \\ &+ \mu_Y\delta_{XZ}(A_X + A_Z)\mu_Y\delta_{XZ} \\ &-1/2\delta_{XYZ}(A_X + A_Y + A_Z)\delta_{XYZ}\}\phi , \end{aligned} \qquad (11)$$

where

$$A_X = \rho h(g^{11} - U^2/a^2),$$
$$A_Y = \rho h(g^{22} - V^2/a^2), \qquad (12)$$
$$A_Z = \rho h(g^{33} - W^2/a^2),$$

are the coefficients of ϕ_{XX}, ϕ_{YY}, and ϕ_{ZZ}, in the expanded form of Eq.(5). Here g^{ij} are the elements of the inverse of the metric tensor G^{-1}, and a^2 is the square of the local speed of sound. The addition of T to Eq.(5) provides recoupling for $0 \leq \varepsilon \leq 1/2$. For $\varepsilon = 1/2$, this reduces Eq.(9) to the usual second-order accurate, six-point Laplacian operator for incompressible flow on a uniform grid.

The scheme is stabilized in supersonic regions by the explicit addition of an artificial viscosity. The viscosity terms added in the original formulation are chosen to emulate the directional bias introduced by the rotated difference scheme of Jameson.[4] The fluxes $\hat{P}$, $\hat{Q}$, and $\hat{R}$ are defined such that

$$\hat{P}_{i,j,k} = \rho h\sigma/a^2(U^2\delta_{XX} + UV\delta_{XY} + UW\delta_{XZ})\phi,$$
$$\hat{Q}_{i,j,k} = \rho h\sigma/a^2(UV\delta_{XY} + V^2\delta_{YY} + VW\delta_{YZ})\phi, \qquad (13)$$
$$\hat{R}_{i,j,k} = \rho h\sigma/a^2(UW\delta_{XZ} + VW\delta_{YZ} + W^2\delta_{ZZ})\phi,$$

where the switching function

$$\sigma = \max(0., 1 - (M_c/M)^2) \qquad (14)$$

is non-zero only for values of the local Mach number M greater than some critical Mach number M_c. Then, after defining

$$P_{i+1/2,j,k} = \begin{cases} \hat{P}_{i,j,k}, & U \geq 0, \\ -\hat{P}_{i+1,j,k}, & U < 0, \end{cases} \qquad (15)$$

with similar shifts for Q and R, Eq.(9) is represented as

$$\delta_X(\mu_{YZ}(\rho hU) + P) + \delta_Y(\mu_{XZ}(\rho hV) + Q) + \delta_Z(\mu_{XY}(\rho hW) + R) + T = 0. \qquad (16)$$

The difference Eqs.(9) approximate the original differential Eq.(5) to within a formal truncation error of second order in the mesh spacing in the physical plane when the mesh is smooth. Since the additional fluxes P, Q, and R added in supercritical regions are of the order of the physical mesh spacing itself, however, Eqs.(16) approximate Eq.(5) to within a truncation error of only first order in the mesh spacing. The error resulting from the introduction of the artificial viscosity can be reduced to second order nearly everywhere in the flow field if we define[6]

$$\nu_{i,j,k} = 1 - \kappa\delta_X\mu_{YZ}\rho \qquad (17)$$

where κ is a constant of order unity, and

$$P_{i+1/2,j,k} = \begin{cases} \hat{P}_{i,j,k} - \nu_{i,j,k}\hat{P}_{i-1,j,k}, & U \geq 0, \\ -\hat{P}_{i+1,j,k} + \nu_{i+1,j,k}\hat{P}_{i+2,j,k}, & U < 0, \end{cases} \qquad (18)$$

Similar expressions are used for the contributons from the Q and R fluxes. In regions where the solution is smooth, the term $\kappa\delta_X\mu_{YZ}\rho$ is of first order in the mesh spacing, and the viscosity is formally a second order quantity. Near a shock, for an appropriate value of κ, the quantity $\nu_{i,j,k}$ becomes small, and Eqs.(18) approximate Eqs.(15) -- i.e., the viscosity reverts to the original first-order form. This hybridization of the second-order scheme has been found necessary to stabilize computations for solutions containing strong shocks.

B. Multi-Grid Iteration

The difference equations resulting from Eq.(16) can be solved by carefully constructed SLOR schemes. The SLOR schemes described in References 1-3 were constructed in a manner that required only tridiagonal inversions along each line. When the contributions arising from the inclusion of the artificial viscosity terms are included, the corrections at each point are coupled to those of its two neighbors on one side (either side must be allowed in a general scheme, depending upon the sign of the velocity) for the first-order scheme, and its three nearest neighbors on one side for the second-order form of the viscosity. Thus, a general scheme which accounts for all these contributions would require a pentadiagonal inversion for the first-order scheme, or a septadiagonal inversion for the second-order scheme. It was found that the pentadiagonal inversion scheme was substantially more stable than the tridiagonal scheme when the second-order form of the viscosity was used, but made little difference in convergence behavior when the first-order viscosity was used. Complementary experiments by A. Jameson of Princeton University have shown no consistent advantage in using septadiagonal inversions (over the pentadiagonal scheme) when the second-order viscosity is used. The pentadiagonal inversion scheme has been incorporated for the present calculations.

Both X-line and Y-line schemes have been implemented. Only the Y-line scheme will be described here; the X-line scheme can be similarly constructed. Also, the coefficients will be described only for the case when $U,V,W > 0$; the coefficients for other cases can easily be constructed by analogy.

We define

$$A_U = \omega_s\rho hU/a^2 \max(|U|, |V|, |W|),$$
$$A_V = \omega_s\rho hV/a^2 \max(|U|, |V|, |W|), \qquad (19)$$
$$A_W = \omega_s\rho hW/a^2 \max(|U|, |V|, |W|),$$

where ω_s is a parameter governing the amount of ϕ_{st} type damping added explicitly to the time

dependent equation modelling the relaxation process. Also,

$$A_{UU} = \rho h \sigma U^2/a^2,$$
$$A_{VV} = \rho h \sigma V^2/a^2, \qquad (20)$$
$$A_{WW} = \rho h \sigma W^2/a^2.$$

Then the correction to the potential

$$C_{i,j,k} = \phi^{(n+1)}_{i,j,k} - \phi^{(n)}_{i,j,k}, \qquad (21)$$

is calculated according to

$$\begin{aligned}
&(A_Y + A_V)(C_{i,j,k} - C_{i,j-1,k}) \\
&+ (A_Z + A_W)(C_{i,j,k} - C_{i,j,k-1}) \\
&+ (A_X + A_U)(C_{i,j,k} - C_{i-1,j,k}) \\
&\quad + A_X (C_{i,j,k} - C_{i+1,j,k}) \\
&+ A_{UU}\{-C_{i+1,j,k} + (3 + \nu_{i,j,k})C_{i,j,k} \qquad (22)\\
&\quad - (3 + 2\nu_{i,j,k} + \nu_{i-1,j,k})C_{i-1,j,k} \\
&\quad + (1 + \nu_{i,j,k} + \nu_{i-1,j,k})C_{i-2,j,k}\} \\
&+ A_{VV}\{(3 + \nu_{i,j,k})C_{i,j,k} - (4 + 3\nu_{i,j,k})C_{i,j-1,k} \\
&\quad + (1 + 2\nu_{i,j,k})C_{i,j-2,k}\} \\
&+ A_{WW}\{(3 + \nu_{i,j,k})C_{i,j,k} - (3 + \nu_{i,j,k})C_{i,j,k-1}\} \\
&\quad + (2/\omega - 1)(A_Y + A_Z)C_{i,j,k} = -R_{i,j,k}
\end{aligned}$$

where $R_{i,j,k}$ is the residual of Eq.(16), calculated using values of the potential from the previous iteration, and ω is an overrelaxation parameter, which is set to 2 in supersonic regions. Eq.(22) requires a pentadiagonal inversion along each i-line since for $U < 0$ the formula must be modified to include the effect of the correction at the (i+2,j,k) point. The V and W components should be non-negative in supersonic zones for the relaxation sweeps to proceed in the positive Y- and Z- directions. Note that the influence of corrections at the (i,j+1,k) and (i,j,k+1), (i,j,k-2) points as well as the (i-3,j,k), (i,j-3,k) and (i,j,k-3) points have been eliminated by the effective addition of mixed space-time differences.

These SLOR schemes have the advantages of being quite stable, and of rapidly eliminating any large local errors in the initial estimates for the potential field. Their rates of convergence decrease as the local errors become smaller, however, with the result that convergence to very small residuals can be excruciatingly slow, especially when the mesh spacing is small.

An efficient alternative has been demonstrated by Jameson,[6] based upon the multi-level adaptive-grid technique first proposed by Fedorenko,[4] and developed and popularized by Brandt.[5] The concept behind the multi-grid method is to eliminate each band of wavenumbers in the error spectrum on a finite-difference grid which is, in a sense, optimal for that component. Thus, low wavenumber errors are eliminated on coarse grids, and only the high wavenumber components need be eliminated on the fine grids. Alternatively, the use of coarse grids to eliminate the low wavenumber component of the error can be thought of as allowing a very high signal speed for the effects of this error to be transmitted across the grid.

The multi-grid method was first applied to the transonic small disturbance equation by South and Brandt,[9] who noted the problems associated with highly stretched grids when using SLOR as the smoothing algorithm, and suggested using alternating SLOR as a remedy. Three-dimensional calculations using the full potential equation (in non-conservation form) have been performed by McCarthy and Reyhner,[10] for the transonic flow past axisymmetric inlets. Their computations were performed in a non-body-aligned, cylindrical coordinate system.

The structure of the multi-grid method is as follows. Let the discretization of Eq.(16) be represented by

$$L^k\phi^{(n+1)} = F^k, \qquad k=1,2,\ldots,K, \qquad (23)$$

on a heirarchy of grid levels $G^0, G^1, \ldots, G^K$, with K denoting the finest grid. The iterative solution is started from some initial estimate on the finest grid. After the high wavenumber component of the error has been eliminated, the fine-grid residual is calculated and restricted to the next coarsest grid. On all but the finest grid, the residual must be modified to account for the difference in truncation error on the various grid levels (i.e., $L^k\phi \neq 0$ unless $k = K$, where ϕ is the converged solution on the K-th grid). Thus

$$F^{k-1} = L^{k-1}\phi^{(n)} - I^{k-1}_k L^k \phi^{(n)}, \qquad (24)$$

where I^{k-1}_k is a restriction operator which averages the residuals over the fine mesh points in the vicinity of each coarse grid point. After the high wavenumber error on the coarser grid has been eliminated, the finer mesh solution can be improved according to

$$\phi^{(n+1)} = \phi^{(n)} + I^k_{k-1}(\phi^{(n+1)} - \phi^{(n)}), \qquad (25)$$

where I^k_{k-1} is a prolongation operator which is used to interpolate the coarse grid corrections onto the finer grid.

While the essence of the idea has been described above for two grid levels, the idea can be extended to as many levels as feasible in order to work on the broadest possible band of the error wavenumber spectrum. Useful error reduction can be achieved on very coarse grids, containing only a few cells in each coordinate direction.

In the original implementation of Brandt,[5] an adaptive strategy was envisioned for determining when to change from one grid level to the next. The smoothing would continue on a particular grid level until the convergence rate fell below some predetermined tolerance, at which time the residual from that grid would be restricted to the next coarsest grid. The smoothing on that grid would proceed until the convergence rate again slowed, at which time the residual would again be restricted to a coarser grid, and the process repeated. When the solution had converged on the coarsest level, the corrections would successively be added back to the finer grid solutions, and the cycle would be repeated. In the present implementation, a simple fixed strategy has been found effective. A fixed number of relaxation sweeps is performed on each grid before restricting the residual from that grid to the next coarsest level, and a fixed number of relaxation sweeps is performed on each grid after the corrections are added from the preceding grid before the corrections are added to the next finest grid.

In the present codes, as in our earlier work,[8] the restriction operator averages the residuals at the 27 fine grid neighbors of each coarse grid point, weighted according to the fraction of the coarse grid cell volume asociated with each fine grid cell in the computational space. The prolongation operator uses four-point Lagrangian interpolation in each coordinate direction, except near boundaries where the order must be reduced.

The computational labor required for one multi-grid cycle using this fixed strategy is as follows. Let one work unit be defined as the labor required for one relaxation sweep on the finest grid. Then if m_1 sweeps are done on each grid before the residual is restricted to the next coarsest grid, and m_2 sweeps are done on each grid before the corrections are prolonged to the next finest grid, then the cost of one complete multi-grid cycle is approximately

$$\{8(m_1 + 1) + m_2\}/7 \quad \text{work units.}$$

This includes the cost of computing the residual on each grid for restriction to the next coarsest grid as approximately equal that of a relaxation sweep on that grid (since most of the labor is involved in computing the residual, not in the actual update of the solution), but neglects the overhead in restricting residuals and prolonging corrections. For $m_1 = m_2 = 1$, one multi-grid cycle requires approximately 2-3/7 work units.

The success of the multiple-grid method depends upon the efficient elimination of high wavenumber errors on any given grid. Jameson[6] used a generalized alternating-direction scheme, in which he replaced the usual constant in each factor by the sum of a constant and first-order difference operators in each coordinate direction. Shmilovich and Caughey[8] have shown that, even for SLOR schemes, the growth factor in a von Neumann analysis should never exceed approximately 0.78 per multi-grid cycle if the multi-grid algorithm is effective on error with low wavenumber components in any of the three coordinate directions. The effectiveness of the multi-grid procedure in eliminating error having low wavenumber component in only one (or two) directions was not verified in the present work, but it was found effective to alternate between X-line and Y-line SLOR in conjunction with the multi-grid procedure. This can be done in two different ways: (1) alternate multi-grid cycles can be performed using the two schemes, or (2) the two schemes can be alternated at each level within each multi-grid cycle (if m_1 and m_2 are greater than one). The most effective procedure seems to be the second option (with $m_1 = 2$ and $m_2 = 4$ or 6).

C. Geometrical Aspects

The algorithm described above has been incorporated into two computer programs for calculating the transonic potential flow past three-dimensional wings and wing-fuselage combinations. These codes are known generally as FLO-27 and FLO-30. FLO-27 analyses the flow past swept wings of essentially arbitrary planform and section shape; FLO-30 analyses the flow past such wings mounted upon arbitrary fuselage shapes.

Both codes construct boundary-conforming coordinate grids by sequences of simple conformal and shearing transformations. The computational domain in each program is terminated at artificial boundaries, located approximately ten chords distant from the wing surface in each spanwise surface, and approximately four semi-spans from the symmetry plane or fuselage in the lateral direction. On the upstream and lateral boundaries, the potential describing perturbations from the uniform free stream is set to zero, while on the downstream boundary, the velocity perturbations in the streamwise direction are set to zero (consistent with a fully-developed flow in the Trefftz plane). The no-flux condition is enforced directly in the flux balances at solid boundaries, and a linearized approximation to the vortex sheet, which assumes the shed vorticity trails in the freestream direction in a fixed surface downstream of the trailing edge is used. The flux balance represented by Eq.(16) is also satisfied at points on the vortex sheet, since it does not require differences across the sheet.

These codes, and their associated grid generation techniques, are described in greater detail in References 1-3.

III. RESULTS

Results will be presented illustrating both the improved rate of convergence of the multi-grid algorithm, and the increased accuracy of the scheme with the second-order viscosity.

A. Computational Aspects

Both programs have been designed to run on either modest computers with large virtual memory or on advanced machines with large high-speed memories. Even so, only the Cartesian

coordinates of the mesh and the solution vector can reasonably be stored for fine meshes, and the transformation derivatives are recomputed at each mesh point in each iteration. Largely because of this, the program runs efficiently on vector machines even though the actual line inversions for the solution are inherently recursive. On a grid containing 160x24x32 mesh cells in the X, Y, and Z directions, respectively, FLO-30 requires about 830,000 words of storage on the Cray-I computer, and requires about 2.0 CPU seconds per work unit on this grid. This corresponds to an estimated average computational rate of 32 megaflops. A typical solution is converged to within reasonable engineering accuracy after about 30 work units; this requires approximately 65 seconds on this (relatively fine) grid.

B. Computed Results

The first results to be presented are for the high-aspect-ratio, supercritical wing (Wing A) tested by Hinson and Burdges.[11] A perspective view of the wing is shown in Figure 2. The flow past the wing at a freestream Mach number of 0.82 and 1.5 degrees angle of attack was analysed using FLO-27. The analysis was performed on a sequence of three grids, each obtained by doubling the number of mesh cells in each coordinate direction from the preceding grid, and prolonging the results of the converged solution from the preceding grid as the initial estimate on the next grid. The finest grid contained 128x16x32 mesh cells. Calculations were performed with both the first- and second-order forms of the artificial viscosity; the iterative convergence rates were nearly identical. Figure 3 shows the convergence history of the second-order scheme on the finest grid. The logarithm of the average residual, the root section lift coefficient, and the number of supersonic points are plotted as a function of computational work (measured in work units); the lift coefficient is normalized by its final converged value, and number of supersonic points is normalized by twice its final converged value, while the residual is normalized by its initial value. The solid lines represent the convergence of the multi-grid algorithm (with $m_1 = 2$, $m_2 = 6$, and the alternating SLOR scheme) using 4 grid levels, and the dashed lines represent the convergence of a relaxation solution for the same initial guess. Note that after even 100 relaxation sweeps, the SLOR scheme has eliminated only about half of the error in root section lift coefficient and in the number of supersonic points. This illustrates the slowness with which SLOR eliminates the low wavenumber component of error. With the multi-grid scheme, both of these measures have converged to within the plottable accuracy of the figure in the equivalent of 50 relaxation sweeps. The wing surface pressure distribution for the first- and second-order accurate schemes are presented in Figures 4(a) and 4(b), and the streamwise pressure distributions at the 25 per cent semi-span station are presented for both schemes in Figures 5(a) and 5(b). Note the increased sharpness with which the shocks are resolved by the higher-order scheme. Finally, a convergence study of the wing lift and drag coefficients with mesh spacing is shown in Figure 6. Both first- and second-order accurate results are plotted; the former *vs.* mesh spacing and the latter *vs.* the square of the mesh spacing. Straight lines through the finer mesh results for both schemes converge to the same asymptotic value for the lift coefficient in the limit of zero mesh width, but the drag results have not yet reached their asymptotic rates on these grids. The absolute error in lift for the second-order scheme on the finest grid is about 2 per cent, while a mesh containing more than eight times as many cells (a factor of 2 in each coordinate direction) would be required for similar accuracy using the first-order scheme. The absolute error in the drag coefficient for the second-order scheme is about 3 per cent, while similar accuracy for using the first-order scheme would seem to require approximately 64 times as many mesh cells (a factor of four in each coordinate direction).

Finally, to illustrate the reliability of the scheme, results for a strongly supercritical case are presented. The flow past the ONERA M-6 wing,[12] mounted upon a circular cylinder, was computed using FLO-30. Figure 7 shows the coordinate lines in the wing and fuselage surfaces for the grid used; only every fourth line is shown for clarity. The solution was computed at a freestream Mach number of 0.923 and 3.06 degrees angle of attack on a very fine grid containing 160x24x32 mesh cells. Nearly 20 per cent of the mesh points have supersonic velocities for this case. The wing pressure distribution, showing the strong shocks at the trailing edge of the upper surface and the substantial supersonic pocket outboard on the lower surface, is plotted in Figure 8. The convergence history is plotted in Figure 9. Again, the root section lift coefficient and the number of supersonic points have converged to within plottable accuracy in the equivalent of about 50 relaxation sweeps.

IV. CONCLUDING REMARKS

A multi-grid algorithm has been combined with a successive-line-overrelaxation (SLOR) iterative scheme to provide improved rates of convergence in the iterative sense for the computation of transonic potential flows past swept wing and wing-fuselage configurations. At the same time, a modified form of artificial viscosity has been incorporated which results in second-order accuracy for the scheme nearly everywhere in the flow field. The method has been incorporated into two computer programs for calculating the transonic potential flow past three-dimensional wings and wing-fuselage combinations. Results indicate that convergence adequate for most engineering purposes can be achieved with the new multi-grid algorithm in less than the time required for about 50 relaxation sweeps using the original SLOR scheme.

V. ACKNOWLEDGEMENTS

This work was supported by the NASA Ames Research Center under Contract NAS-9913, and by the Office of Naval Research under Contract

N00014-77-C-0033. The author would like to acknowledge many fruitful discussions with Professor Antony Jameson of Princeton University during the course of this work, and to thank Mr. Arvin Shmilovich of Cornell University for providing an early version of the multi-grid algorithm for use with FLO-30.

VI. REFERENCES

1. Jameson, Antony and Caughey, D.A., "A Finite-Volume Method for Transonic Potential Flow Calculations," Proc. of AIAA 3rd Computational Fluid Dynamics Conference, pp. 35-54, Albuquerque, N.M., June 27-29, 1977.

2. Caughey, D.A. and Jameson, Antony, "Numerical Calculation of Transonic Potential Flow about Wing-Body Combinations," AIAA Journal Vol. 17, pp. 175-181, February 1979.

3. Caughey, D.A. and Jameson, Antony, "Progress in Finite-Volume Calculations for Wing-Fuselage Combinations," AIAA Journal Vol. 18, pp. 1281-1288, November 1980.

4. Fedorenko, R. P., "A Relaxation Method for Solving Elliptic Difference Equations," USSR Comput. Math. and Math. Phys. Vol. 1, pp. 1092-1096, 1962.

5. Brandt, Achi, "Multi-Level Adaptive Grid Technique (MLAT) for Fast Numerical Solution to Boundary Value Problems," Proc. Third Int'l. Conf. on Numerical Methods in Fluid Mechanics," Paris, 1972, Vol. 1, pp.82-89, Springer, New York, 1973.

6. Caughey, D. A. and Jameson, Antony, "Basic Advances in the Finite-Volume Method for Transonic Potential Flow Calculations," Proc. of Symposium on Numerical and Physical Aspects of Aerodynamic Flows, Long Beach, California, January 1981.

7. Jameson, Antony, "A Multi-Grid Scheme for Transonic Potential Calculations on Arbitrary Grids," Proc. of AIAA 4th Computational Fluid Dynamics Conference, pp. 122-146, Williamsburg, Va., July 23-25, 1979.

8. Shmilovich, A. and Caughey, D. A., "Application of the Multi-grid Method to Calculations of Transonic Potential Flow about Wing-fuselage Combinations," Proc. of NASA Symposium on Multi-grid Methods, NASA Ames Research Center, Moffett Field, California, October 21-22, 1981, NASA CP 2202, pp. 101-130.

9. South, J. C. Jr., and Brandt, Achi, "Application of a Multi-level Grid Method to Transonic Flow Calculations," in Transonic Flow Problems in Turbomachinery, pp. 180-207, T. C. Adamson and M. F. Platzer, Eds. Hemisphere, Washington, D. C., 1977.

10. McCarthy, D. R. and Reyhner, T. A., "Multi-Grid Code for Three-dimensional Transonic Potential Flow about Inlets," AIAA Journ ' Vol. 20, pp. 45-50, January 1980.

11. Hinson, B. L., and Burdges, K. P., "An Evaluation of Three-dimensional Transonic Codes using New Correlation-tailored Test Data," AIAA Paper 80-0003, 13th Aerospace Sciences Meeting, Pasadena, California, January 14-16, 1980.

12. Monnerie, B., et Charpin, F., "Essais de buffeting d'une aile en fleche en transsonique," 10e Colloque d'Aerodynamique Applique, Lille, France, November 1973.

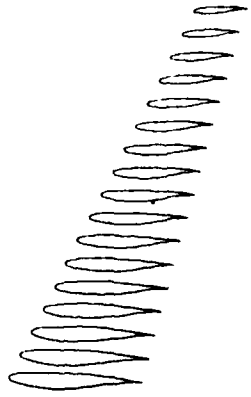

Figure 2. Geometry of Lockheed Wing A; sections at computational stations on fine grid are shown.

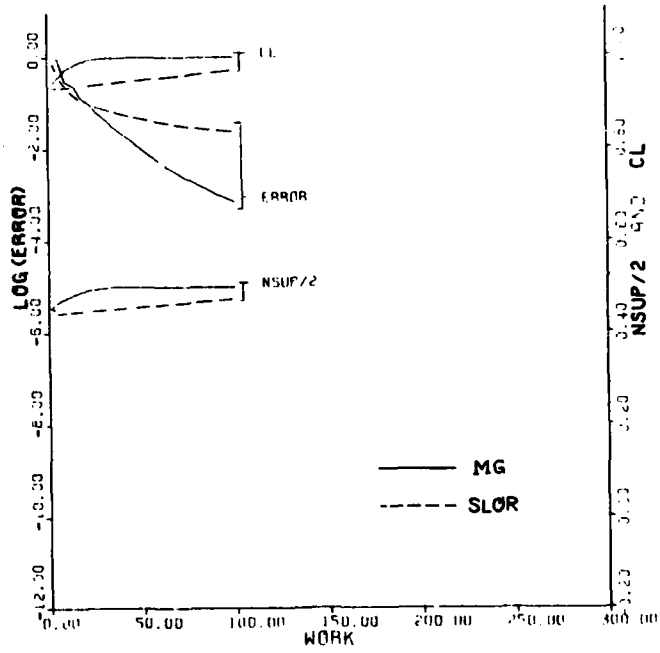

LOCKHEED WING A

MACH	0.820	ALPHA	1.500
RESID1	0.7890-05	RESID2	0.5360-08
WORK	100.47	RATE	0.9300
GRID	128X16X32		

Figure 3. Iterative convergence for calculation of flow past Lockheed Wing A at $M_\infty = 0.82$ and 1.5 degrees angle of attack; second-order scheme.

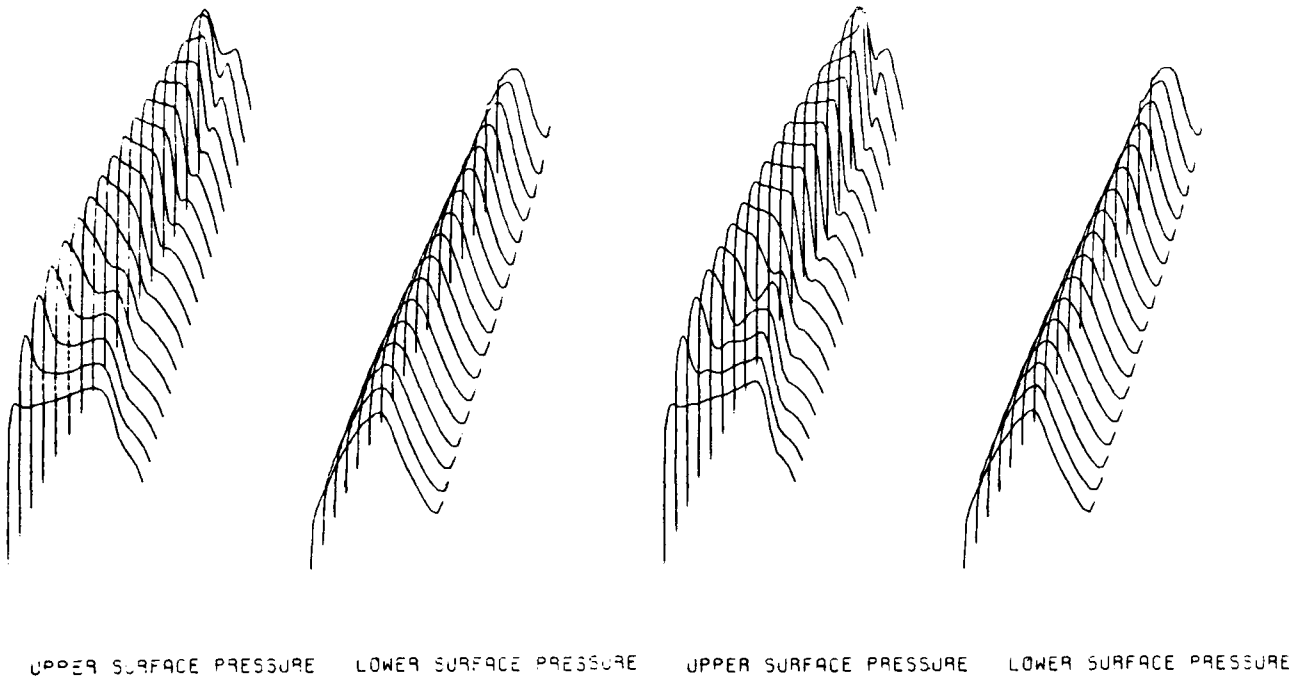

(a) First-order viscosity (b) Second-order viscosity

Figure 4. Three-dimensional wing surface pressure distributions for Lockheed Wing A at M_∞ = 0.82 and 1.5 degrees angle of attack.

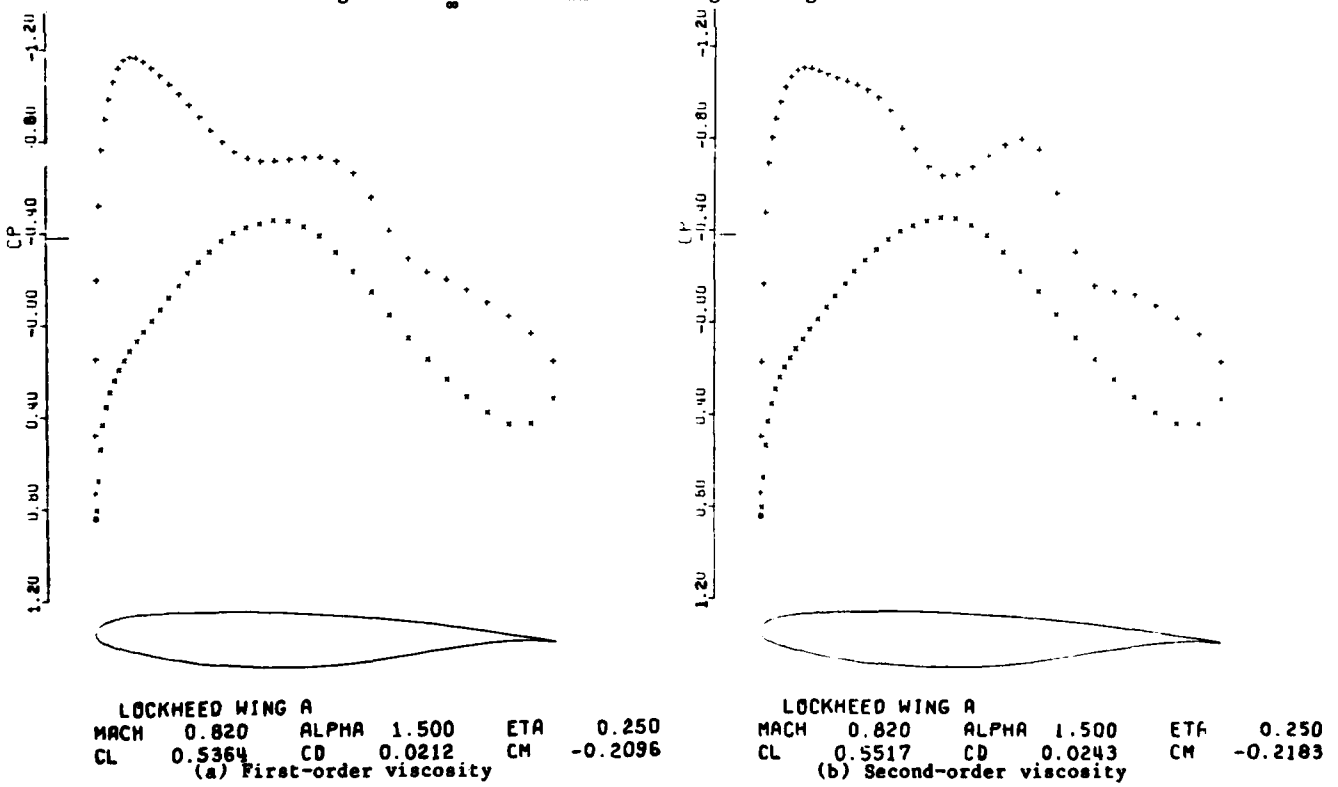

(a) First-order viscosity (b) Second-order viscosity

Figure 5. Streamwise surface pressure distributions for Lockheed Wing A at 25 per cent semi-span station. Same freestream conditions as Figure 4.

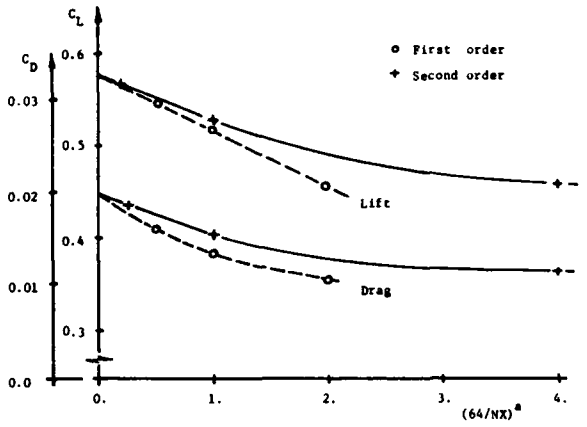

Figure 6. Convergence study of wing lift and drag coefficients for Lockheed Wing A. Same freestream conditions as Figures 4 and 5.

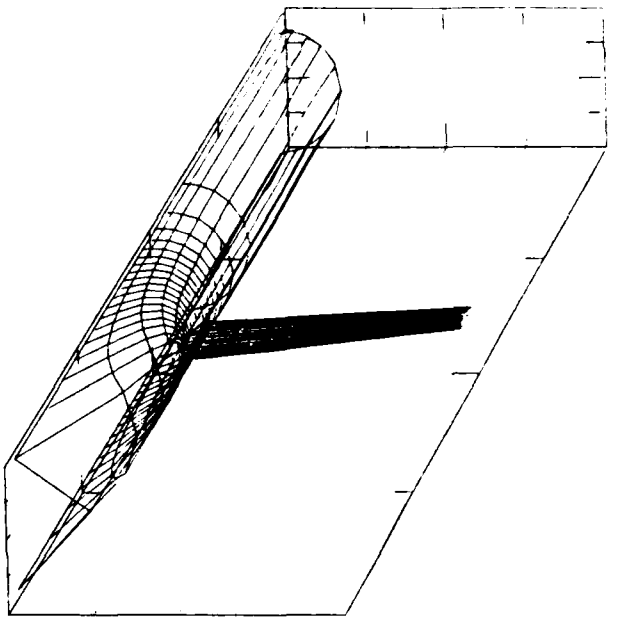

Figure 7. ONERA wing M-6 mounted upon cylindrical fuselage. Grid lines shown in wing and fuselage surfaces only; every fourth line shown.

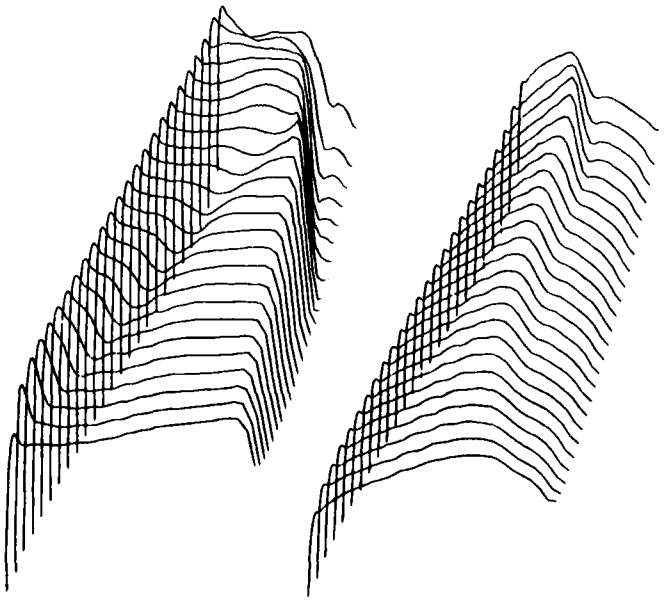

UPPER SURFACE PRESSURE LOWER SURFACE PRESSURE

ONERA WING ON CYLINDRICAL FUSELAGE
MACH 0.923 ALPHA 3.060
CL 0.4779 CD 0.0444 CM -0.4543

Figure 8. Wing surface pressure distribution for flow past ONERA Wing-cylinder combination at M_∞ = 0.923 and 3.06 degrees angle of attack.

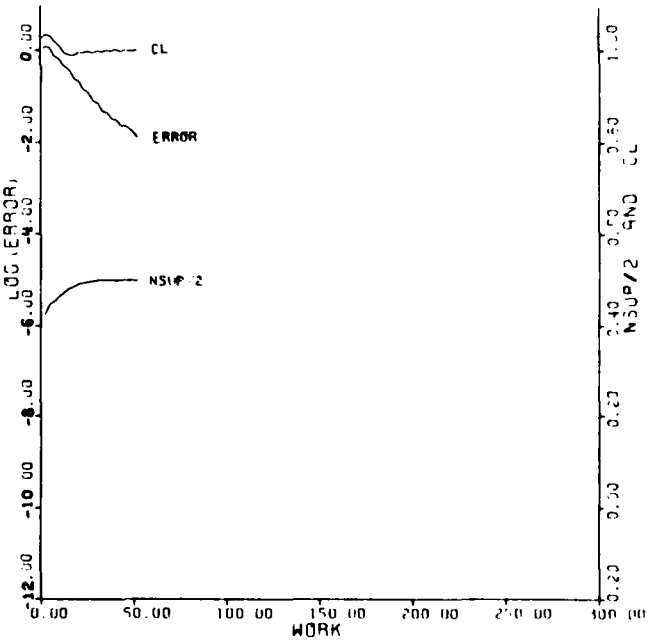

ONERA WING ON CYLINDRICAL FUSELAGE
MACH 0.923 ALPHA 3.060
RESID1 0.5320-04 RESID2 0.6830-06
WORK 52.37 RATE 0.9202
GRID 160X24X32

Figure 9. Iterative convergence for calculation of flow past ONERA wing-cylinder combination. Freestream conditions as in Figure 8.

-- NOTES --

DISTRIBUTION LIST FOR UNCLASSIFIED
TECHNICAL REPORTS AND REPRINTS ISSUED UNDER
CONTACT N00014-77-C-0033 TASK 061-242

Technical Library
Building 313
Ballistic Research Laboratories
Aberdeen Proving Ground,
Maryland 21005

Mr. Aviars Celmins
Ballistic Research Laboratory
Ballistic Modelling Division
Aberdeen Proving Ground,
Maryland 21005

Dr. P. J. Roache
Ecodynamics Research Associates,
Inc.
P. O. Box 8172
Albuquerque, NM 87108

Defense Technical Information
Center
Cameron Station, Building 5
Alexandria, VA 22314

Library
Naval Academy
Annapolis, MD 21402

Director, Tactical Technology
Office
Defense Advanced Research
Projects Agency
1400 Wilson Boulevard
Arlington, VA 22209

Code 200B
Office of Naval Research
800 N. Quincy Street
Arlington, VA 22217

Code 438
Office of Naval Research
800 N. Quincy Street
Arlington, VA 22217

Dr. J. L. Potter
Deputy Director, Technology
von Karman Gas Dynamics Facility
Arnold Air Force Station,
Tennessee 37389

Professor J. C. Wu
School of Aerospace Engineering
Georgia Institute of Technology
Atlanta, GA 30332

Library
Aerojet-General Corporation
6352 North Irwindale Avenue
Azusa, CA 9172

NASA Scientific and Technocal
Information Facility
P. O. Box 8757
Baltimore/Washington
International Airport,
Maryland, 21240

Dr. K. C. Wang
San Diego State University
College of Engineering
San Diego, CA 92182

Professor A. J. Chorin
Department of Mathematics
University of California
Derkeley, CA 94720

Professor M. Holt
Department of Mechanical
Engineering
University of California
Berkelye, CA 94720

Dr. H. R. Chaplin
Code 1600
David W. Taylor Naval Ship
Research and Development
Center
Bethesda, MD 20084

Dr. Hans Lugt
Code 1802
David W. Taylor Naval Ship
Research and Development
Center
Bethesda, MD 20084

Dr. Francois Frenkiel
Code 1802
David W. Taylor Naval Ship
Research and Development
Center
Bethesda, MD 20084

Dr. G. R. Inger
Department of Aerospace
Engineering
Virginia Polytechnic Institu
and State University
Blacksburg, VA 24061

Professor C. H. Lewis
Department of Aerospace and
Ocean Engineering
Virginia Polytechnic Institu
and State University
Balcksburg, VA 24061

Professor A. H. Nayfeh
Department of Engineering
Science
Virginia Polytechnic Institu
and State University
Blacksburg, VA 24061

Dr. A. Rubel
Research Department
Grumman Aerospace Corporatio
Bethpage, NY 11714

Director
Office of Naval Research Eas
Central Regional Office
666 Summer Street, Bldg. 114
Section D
Boston, MA 02210

Dr. J. C. Erickson, Jr.
CALSPAN Corporation
Advanced Technology Center
P. O. Box 400
Buffalo, NY 14225

Dr. T. J. Falk
CALSPAN Corporation
Advanced Technology Center
P. O. Box 400
Buffalo, NY 14225

Dr. C. Witliff
CALSPAN Corporation
Advanced Technology Center
P. O. Box 400
Buffalo, NY 14225

Professor R. F. Probstein
Department of Mechanical
Engineering
Massachusetts Institute of
Technology
Cambridge, MA 02139

Commanding Officer
Office of Naval Research
Branch Office
536 South Clark Street
Chicago, IL 60605

Code 753
Naval Weapons Center
China Lake, CA 93555

Mr. J. Marshall
Code 4063
Naval Weapons Center
China Lake, CA 93555

Professor R. T. Davis
Department of Aerospace Engineering
University of Cincinnati
Cincinnati, OH 45221

Professor S. G. Rubin
Department of Aerospace Engineering and Applied Mechanics
University of Cincinnati
Cincinnati, OH 45221

Library MS 60-3
NASA Lewis Research Center
21000 Brookpark Road
Cleveland, OH 44135

Dr. J. D. Anderson, JR.
Chairman, Department of Aerospace Engineering
College of Engineering
University of Maryland
College Park, MD 20742

Professor O. Burggraf
Department of Aeronautical and Astronautical Engineering
Ohio State University
1314 Kinnear Road
Columbus, OH 43212

Technical Library
Naval Surface Weapons Center
Dahlgren Laboratory
Dahlgren, VA 22448

Dr. F. Moore
Naval Surface Weapons Center
Dahlgren Laboratory
Dahlgren, VA 22448

Technical Library 2-51131
LTV Aerospace Corporation
P. O. Box 5907
Dallas, TX 75222

Library, United Aircarft Corporation Research Laboratory
Silver Lane
East Hartford, CT 06108

Professor G. Moretti
Polytechnic Institute of New York, Long Island Center
Department of Aerospace Engineering and Applied Mechanics
Route 110
Farmingdale, NY 11735

Dr. W. R. Briley
Scientific Research Associates, Inc.
P. O. Box 498
Glastonbury, CT 06033

Professor P. Gordon
Calumet Campus
Department of Mathematics
Purdue University
Hammond, IN 46323

Professor A. Chapmann
Chairman, Mechanical Engineering
William M. Rice Institute
Box 1892
Houston, TX 77001

Technical Library
Naval Ordnance Station
Indian Head, MD 20640

Professor D. A. Caughey
Sibley School of Mechanical and Aerospace Engineering
Cornell University
Ithaca, NY 14853

Professor E. L. Resler
Sibley School of Mechanical and Aerospace Engineering
Cornell University
Ithaca, NY 14853

Professor S. F. Shen
Sibley School of Mechanical and Aerospace Engineering
Cornell University
Ithaca, NY 14853

Library
Midwest Research Institute
425 Volker Boulevard
Kansas City, MO 64110

Dr. M. M. Hafez
Flow Research, Inc.
P. O. Box 5040
Kent, WA 98031

Dr. E. M. Murman
Flow Reserarch, Inc.
P. O. Box 5040
Kent, WA 98031

Kr. J. J. Riley
Flow Research, Inc.
P. O. Box 5040
Kent WA 98031

Dr. S. A. Orzag
Cambridge Hydrodynamics, Inc.
54 Baskin Road
Lexington, MA 02173

Dr. P. Bradshaw
Imperial College of Science a Technology
Department of Aeronautics
Prince Consort Road
London SW7 2BY, England

Professor T. Cebeci
Mechanical Engineering Dept.
California State University, Long Beach
Long Beach, CA 90840

Dr. H. K. Cheng
University of Southern California
Department of Aerospace Engr.
University Park
Los Angeles, CA 90007

Dr. D. R. Kotansky
Department 341
P. O. Box 516
St. Louis, MO 63166

Dr. Charles Watkins
Mechanical Engineering Dept.
Howard University
Washington, DC 20059

Professor J. C. Cole
Mechanics and Structures Dept.
School of Engineering and
Applied Science
University of California
Los Angeles, CA 90024

Engineering Library
University of Southern
California
Box 77929
Los Angeles, CA 90007
Dr. C. M. Ho
Department of Aerospace
Engineering
University of Southern Calif.
University Park
Los Angeles, CA 90007
Dr. T. D. Taylor
The Aerospace Corporation
P. O. Box 92957
Los Angeles, CA 90009

Commanding Officer
Naval Ordnance Station
Louisville, KY 40214

Mr. B. H. Little, Jr.
Lockheed-Georgia Company
Department 72-74, Zone 369
Marietta, GA 30061

Professor E. R. G. Eckert
University of Minnesota
241 Mechanical Engineering
Building
Mineapolis, MN 55455

Dr. Gary Chapman
Mail Stop 227-4
Ames Research Center
Moffett Field, CA 94035

Library
Naval Postgraduate School
Monterey, CA 93940

Dr. J. L. Steger
Flow Simulations, Inc.
735 Alice Avenue
Mountain View, CA 94041

Engineering Societies Library
345 East 47th Street
New York, NY 10017

Professor G. Miller
Department of Applied Science
New York University
26-36 Stuyvesant Street
New York, NY 10003

Professor A. Jameson
Courant Institute of
Mathematical Sciences
New York University
251 Mercer Street
New York, NY 10012

Office of Naval Research
New York Area Office
715 Broadway - 5th Floor
New York, NY 10003

Dr. A. Vaglio-Laurin
Department of Applied Sciences
New York University
26-36 Stuyvesant Street
New York, NY 10003

Mr. D. Farmer
Naval Ocean Research and
Development Activity
Code 332
NSTL Station, MS 39522

Librarian, Aeronautical Library
National Research Council
Montreal Road
Ottawa 7, Canada

Lockheed Missiles and Space
Company
Technical Information Center
3251 Hanover Street
Palo Alto, CA 94304
Director
Office of Naval Research
Western Regional Office
1030 East Green Street
Pasadena, CA 91106

Engineering Division
California Institute of
Technology
Pasadena, CA 91109

Library
Jet Propulsion Laboratory
4800 Oak Grove Drive
Pasadena, CA 91103

Professor H. Liepmann
Department of Aeronautics
California Institute of
Technology
Pasadena, CA 91109
Mr. L. I. Chasen, MGR-MSD Lib.
General Electric Company
Missile and Space Division
P. O. Box 8555
Philadelphia, PA 19101

Telephonical Library
Naval Missile Center
Point Mugu, CA 93042

Professor S. Bogdonoff
Gas Dynamics Laboratory
Department of Aerospace and
Mechanical Sciences
Princeton University
Princeton, NJ 08540
Professor S. I. Cheng
Department of Aerospace and
Mechanical Sciences
Princeton University
Princeton, NJ 08540

Dr. J. E. Yates
Aeronautical Research Associat
of Princeton, Inc.
50 Washington Road
Princeton, NJ 08540

Professor L. Sirovich
Division of Applied Mathematic
Brown University
Providence, RI 02912

Redstone Scientific Informatio
Center
Chief, Document Section
Army Missile Command
Redstone Arsenal, AL 35809

U. S. Army Research Office
P. O. Box 12211
Research Triangle, NC 27709

Editor, Applied Mechanics Review
Southwest Research Institute
8500 Culebra Road
San Antonio, TX 78228

Library and Information Services
General Dynamics-CONVAIR
Kearny Mesa Plant
P. O. Box 80847
San Diego, CA 92138

Office of Naval Research
San Francisco Area Office
One Hallidie Plaza, Suite 601
San Francisco, CA 94102

Library
The RAND Corporation
1700 Main Street
Santa Monica, CA 94102

Dr. P. E. Rubbert
Boeing Aerospace Company
Boeing Military Airplane
Development Organization
P. O. Box 3707
Seattle, WA 98124

Librarian
Naval Surface Weapons Center
White Oak Laboratory
Silver Spring, MD 20910

Dr. J. M. Solomon
Naval Surface Weapons Center
White Oak Laboratory
Silver Spring, MD 20910

Professor J. H. Ferziger
Department of Mechanical
Engineering
Stanford University
Stanford, CA 94305

Professor K. Karamcheti
Department of Aeronautics and
Astronautics
Stanford University
Stanford, CA 94305

Professor O. Bunemann
Institute for Plasma Research
Stanford University
Stanford, CA 94305

Engineering Library
McDonnell Douglass Corporation
Department 218, Building 101
P. O. Box 516
St. Louis, MO 63166

Dr. N. Malmuth
Rockwell International Science
Center
1049 Camino Dos Rios
P. O. Box 1085
Thousand Oaks, CA 91360

Library
Institute of Aerospace Studies
University of Toronto
Toronto 5, Canada

Professor W. R. Sears
Aerospace and Mechanical Engr.
University of Arizona
Tucson, AZ 85721

Professor A. R. Seebass
Department of Aerospace and
Mechanical Engineering
University of Arizona
Tucson, AZ 85721

Dr. K. T. Yen
Code 3015
Naval Air Development Center
Warminster, PA 18974

Air Force Office of Scientific
Research (SREM)
Building 1410, Bolling AFB
Washington, DC 20332

Library of Congress
Science and Technology Division
Washington, DC 20540

Director of Research (Code RR)
National Aeronautics and Space
Administration
600 Independence Avenue, SW
Washington, DC 20546

Library
National Bureau of Standards
Washington, DC 20234

National Science Foundation
Engineering Division
1800 G Street, NW
Washington DC 20550

AIR 320D
Naval Air Systems Command
Washington, DC 20361

AIR 950D
Naval Air Systems Command
Washington, DC 20375

Code 2627
Naval Research Laboratory
Washington, DC 20375

SEA 03512
Naval Sea Systems Command
Washington, DC 20362

Sea 09G3
Naval Sea Systems Command
Washington DC 20362

Dr. A. L. Slafkosky
Scientific Advisor
Commandant of the Marine Cor
(Code AX)
Washington, DC 20380

Director
Weapons Systems Evaluation
Group
Washington, DC 20350

Research Library
AVCO Corporation
Missile Systems Division
201 Lowell Street
Wilmington, MA 01887

AFAPL (APRC)
AB
Wright Patterson AFB, OH 45

Dr. Donald J. Harney
AFFDL/FX
Wright Patterson AFB, OH 45

END

FILMED

6-83

DTIC